MOEM

Modern Electronic Materials 2024; 10(3): 159–165
DOI 10.3897/j.moem.10.3.140732

Research Article

Thermovoltaic response in two-layered thin-film zinc oxide structures

Vladimir A. Makagonov[1], Konstantin S. Gabriel's[1], Yuri E. Kalinin[1], Artem Yu. Lopatin[1], Ludmila A. Bliznyuk[2], Alexander K. Fedotov[3]

1 *Voronezh State Technical University, 84 20 letiya Oktyabrya Str., Voronezh 394006, Russian Federation*

2 *Scientific-Practical Materials Research Centre of the National Academy of Sciences of Belarus, 19 P. Brovka Str., Minsk 220072, Republic of Belarus*

3 *Belarusian State University, 4 Nezavisimosti Ave., Minsk 220030, Republic of Belarus*

Corresponding author: Artem Yu. Lopatin (lopatin-ayu@mail.ru)

Received 21 March 2024 ♦ **Accepted** 11 July 2024 ♦ **Published** 10 October 2024

Citation: Makagonov VA, Gabriel's KS, Kalinin YuE, Lopatin AYu, Bliznyuk LA, Fedotov AK (2024) Thermovoltaic response in two-layered thin-film zinc oxide structures. *Modern Electronic Materials* 10(3): 159–165. https://doi.org/10.3897/j.moem.10.3.140732

Abstract

A method of measuring the thermovoltaic effect in heterogeneous media with gradient doping impurity distributions producing gradient carrier distributions has been proposed. Iron doped zinc oxide specimens have been produced using ion beam sputtering on thin foil tantalum substrates for thermovoltaic effect measurements, glass-ceramic substrates for Hall measurements and silicon substrates for structural study. The doping impurity concentration x_{Fe} in the specimens has been varied from 0.34 to 4.18 at.%. X-ray phase analysis has shown that all the specimens have a hexagonal zinc oxide crystal structure. The films have preferential [002] orientation. The carrier concentration in the experimental specimen layers according Hall data obtained on an ECOPIA 5500 measurement system in a 0.5 T DC magnetic field has varied in the 10^{16}–10^{20} cm^{-3} range. The specimens have an *n*-type conductivity. Thermovoltaic measurements have been carried out for two-layered iron doped zinc oxide specimens with different carrier and iron doping impurity concentrations using the method proposed. The maximum thermovoltaic response ($U \sim 80$ μV) has been observed in the two-layered thin-film specimen with the carrier concentration difference between the layers ($\Delta n \approx 2 \cdot 10^3$ cm^{-3}). The observed saturation of the thermovoltaic response has been attributed to the establishment of dynamic equilibrium between carrier diffusion from the high carrier concentration layer to the low carrier concentration layer and carrier drift due to internal electric field.

Keywords

thermovoltaic effect, zinc oxide, doping impurity

1. Introduction

Thermovoltaic converters have recently attracted great interest in electric power generation. The thermovoltaic effect (TVE) is spontaneous generation of electromotive force (emf) in gradient-doped semiconductor materials upon uniform heating [1–3]. The fundamental difference between the TVE and the classical Seebeck effect is that the TVE originates not from a temperature gradient but from a chemical potential gradient produced by an impurity concentration gradient and hence a carrier concentration gradient. Then thermal energy is converted to electric power upon uniform specimen heating, i.e., in the absence of a temperature gradient.

In Russia, this effect was first discovered and studied for semiconducting samarium sulfide [3–11]. The TVE mechanism according to the Authors [10] is as follows. Excess Sm^{2+} ions in interstitial positions of the lattice generate a shallow $E_i \sim 45$ meV donor level with a high carrier concentration, $n \sim 10^{20} \div 10^{21}$ cm^{-3}. Temperature growth to a critical level near 400 K thermally activates the carriers at that level thus increasing their concentration in the conduction band. At $T \sim 400$ K, the concentration n becomes sufficient for the complete delocalization of electrons from the E_i level in some local regions due to the screening of the electric potential of the impurity. This delocalization is accompanied by an abrupt surge of the carrier concentration in the conduction band causing Mott's transition in the abovementioned local regions. Those nonequilibrium electrons have a concentration gradient which produces a chemical potential gradient which in turn triggers their diffusion from high carrier concentration regions to low carrier concentration regions thus producing a voltage. This complex process is maintained by permanent heating and can continue for an arbitrary long time. Later on, the presence of thermovoltaic response was also confirmed for homogeneous junctions in zinc oxide doped with variable valence impurities such as iron and copper [1].

As indicated earlier [13], TVE based thermoelectric heat power converters should have numerous advantages upon uniform heating of a semiconducting material: no need to produce a temperature gradient, higher conversion efficiency, lower specific weight etc. From the physical viewpoint, a temperature gradient required for thermoelectric heat power conversion in TVE based generators can be replaced for an impurity concentration gradient (e.g. its inhomogeneous distribution) in a semiconducting thermoelectric material of *n*- or *p*-conductivity type. Gradient TVE structures can be synthesized in bulk semiconductors but batch fabrication of batteries might face problems. However, the synthesis of TVE based thermoelectric heat power converters can be implemented through a relatively small number of process operations if a thin-film technology is used.

Studies of TVE in gradient materials face difficulties in maintaining a constant temperature in the whole test specimen bulk for avoiding the effect of thermo-emf on the measurement results. Taking into account the above, a TVE measurement method was proposed and TVE was measured in two-layered zinc oxide structures with different carrier concentrations in the layers. Zinc oxide was chosen as the test material since polycrystalline zinc oxide has high thermo-emf, low thermoelectric quality (ZT) due to low carrier concentrations (and hence low conductivity) and high heat conductivity coefficient [14–16]. The synthesis and study of thin-film zinc oxide is furthermore of great scientific importance since due to its good transparency and high electron mobility it finds new applications in transparent electrodes for LCDs [14], gas sensors [15], thin-film transistors and LEDs [16] and other devices [17]. The synthesis and stabilization of nanostructures with preset properties is a complex task since nanosized materials have large surface area and high reactivity. Therefore the choice of a synthesis process plays an important role in the formation of nanostructures with required parameters such as crystallite sizes and their distribution, shape, homogeneity etc. Correct process choice can deliver practically applicable materials.

There are various zinc oxide thin film and coating synthesis methods: chemical vacuum deposition [21], electrochemical deposition [22], molecular beam epitaxy [23], pyrolysis [24], vapor phase deposition with thermal [25], pulse laser [26], magnetron [27] and carbothermal sputtering [28], pyrolysis of thiourea coordination compound aerosols onto heated substrates (spray method) [29], low pressure chemical vapor phase deposition (CVD) [30].

Below we consider ion beam sputtering synthesis of $Zn_{1-x}Fe_xO$ films with different carrier concentrations, TVE measurement method developed herein and experimental data on the structural, optical and thermal properties that are important for practical applications.

2. Experimental

The test specimens were synthesized by ion beam sputtering in an UVN-2M vacuum plant described in detail earlier [31]. The substrates were thin foils of tantalum (two-layered specimens to TVE measurement), glass-ceramic (single-layered specimens to Hall measurements) and silicon to structural studies. The bottom layers of the two-layered structures with different iron contents were synthesized by sputtering a water-cooled target consisting of ZnO ceramic base with nonuniformly arranged Fe_2O_3 plates. This method allows synthesizing specimens with different doping element (Fe) concentrations during single deposition process cycle. The top layers of the two-layered structures were deposited from pure ZnO ceramic target. The thickness of the films as measured with a MII-4 interferometer was ~0.75 μm per each layer. The Fe content x_{Fe} in the specimens as measured using the selected area electron probe method ranged from 0.34 to 4.18 at.%. It should be noted that the pure ZnO layers contained small Fe quantities due to specific issues of the ion beam sputtering process.

The structure and phase composition of the specimens were studied using X-ray phase analysis. The measurements were carried out on a Bruker D2 Phaser diffractometer ($\lambda_{CuK\alpha 1}$ = 0.154 nm). The diffraction patterns were analyzed with the DIFFRAC.EVA 3.0 software and the ICDD PDF Release 2012 database [32].

The carrier concentration in the specimen layers was measured using the Hall method on an ECOPIA 5500 measurement system in a 0.5 T DC magnetic field. The Hall specimens were squared, 8×8 mm^2, with ultrasonically soldered indium contacts.

X-ray phase analysis data for ZnO:Fe films with different Fe concentrations are shown in Fig. 1. Analysis of

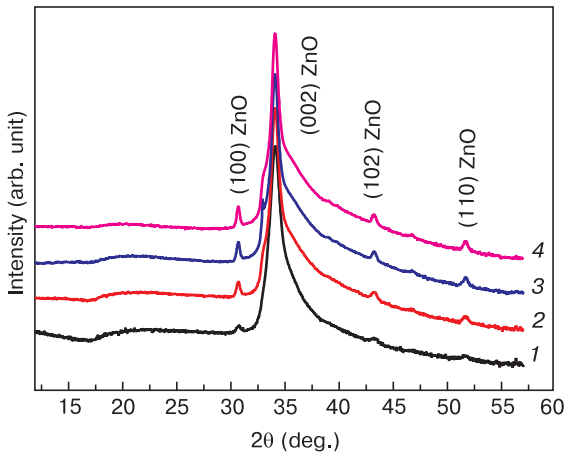

Figure 1. X-ray diffraction patterns of ZnO:Fe films with different Fe concentrations x_{Fe} (at.%): (*1*) 2.85, (*2*) 3.78, (*3*) 4.12, (*4*) 4.91

the diffraction patterns showed that all the specimens had a hexagonal zinc oxide structure. Similar data were obtained earlier for iron doped zinc oxide [33]. The films had preferential [002] orientation.

The thermovoltaic effect was measured on a Netzsch SBA 458 thermo-emf coefficient and specific electrical conductivity measurement system. Figure 2 shows schematic of the measurement cell. The cell is placed in an electric furnace for measurements. A two-layered zinc oxide specimen is installed in the center of the measurement cell on ceramic supports. One layer of the specimen is heavily ion doped (brown). Micro-heaters (red) are installed inside the Al_2O_3 ceramic specimen supports at two sides. Two alumel-chromel (K-type) thermocouples and two current probes for Seebeck coefficient and electrical conductivity measurement respectively are connected to the bottom specimen surface. The thermocouples and the current probes are secured in the ceramic specimen supports. Springs exert a constant load on the thermocouples and the current probes in the cold part of the measurement cell. A pressure pad and an additional load press the specimen to the specimen supports with a constant force.

The entire measurement procedure is automatic and is implemented as follows. The specimen is heated in accordance with the preset stepwise temperature program. Upon reaching the required isothermal exposure temperature T the Seebeck coefficient was measured and then the TVE was measured following the method described below. A temperature gradient was produced for TVE measurement by heating the right-hand side and cooling the left-hand side of the specimen. Then the $U_1 = f(\Delta T)$ curve was recorded where U_1 is the voltage measured relative to the respective branches of the chromel thermocouples. Then a temperature gradient was produced by heating the left-hand side and cooling the right-hand side of the specimen. Then the $U_2 = f(\Delta T)$ curve was recorded where U_2 is the voltage measured relative to the respective branches of the alumel thermocouples. The next stage was plotting linear functions for the resultant $U = f(\Delta T)$ curves (Fig. 3). The TVE voltage was calculated as the arithmetical mean of the data at the $\Delta T = 0$ point of the U_1 and U_2 linear functions of ΔT, i.e., at a zero temperature difference (Fig. 3).

The TVE measurement process described above was used at all the preset temperature steps. It can be seen from Fig. 3 that if this method is used for measuring a uniform specimen (the Ta foil) without temperature gradients, the voltages at the respective thermocouple branches are zero (Fig. 3, curves *3* and *4*), i.e., there is no TVE response. The situation is quite different for a two-layered ZnO/ZnO:Fe specimen (Fig. 4, curves *1* and *2*): the respective thermocouple branches intersect at one point $U = 2.9 \cdot 10^{-5}$ V at a temperature difference of $\Delta T = 0$, i.e., the specimen exhibits the TVE.

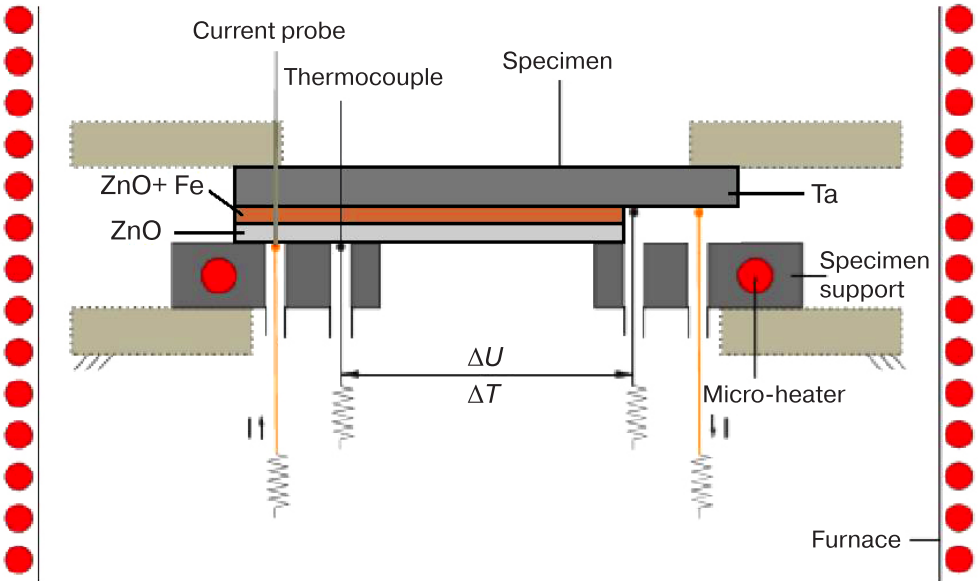

Figure 2. Schematic of measurement cell

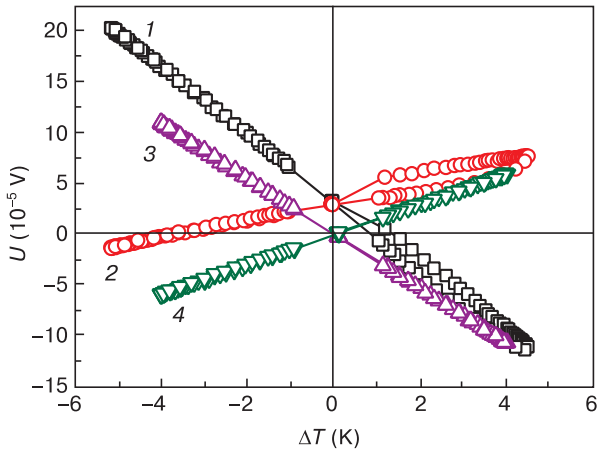

Figure 3. Illustration of TVE response measurement in two-layered thin-film zinc oxide specimens: (*1*, *2*) voltage relative to branches of chromel (U_1) and alumel (U_2) thermocouples, respectively (layer 1 (bottom) x_{Fe} = 0.47 at.% and layer 2 (top) x_{Fe} = 4.18 at. %); (*3*, *4*) voltage relative to branches of chromel (U_1) and alumel (U_2) thermocouples, respectively, for a uniform specimen (Ta foil). Isothermal exposure temperature T = 373 K

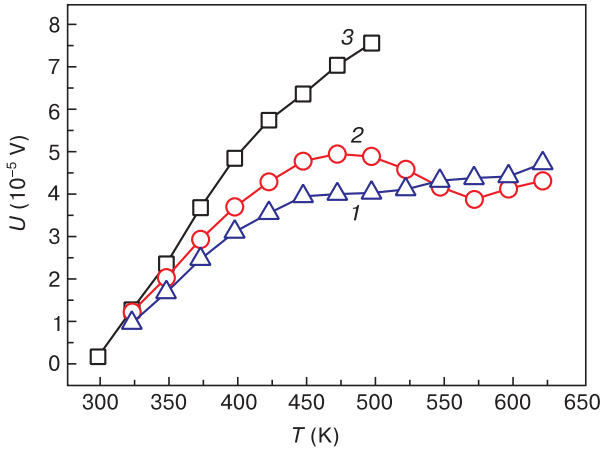

Figure 4. TVE response voltage as a function of temperature for two-layered thin-film ZnO/ZnO:Fe specimens with different iron concentrations: (*1*) specimen 1: layer 1 x_{Fe} = 0.34 at.%, layer 2 x_{Fe} = 4.00 at.%; (*2*) specimen 2: layer 1 x_{Fe} = 0.47 at.%, layer 2 x_{Fe} = 4.18 at.%; (*3*) specimen 3: layer 1 x_{Fe} = 0.55 at.%, layer 2 x_{Fe} = 2.18 at.%

3. Results and discussion

Figure 4 shows TVE response voltage as a function of temperature for two-layered specimens the top layers of which contained different iron concentrations (see Fig. 2). With an increase in temperature the TVE response voltage grows due to an increase in the iron concentration in the undoped (top) layer. At about 423 K the first and second specimens undergo saturation whereas the third specimen (with lower iron concentration in the top layer) is not saturated. To understand the cause of this difference in TVE voltage behavior we measured Hall temperature curves for separate layers of the multilayered structures

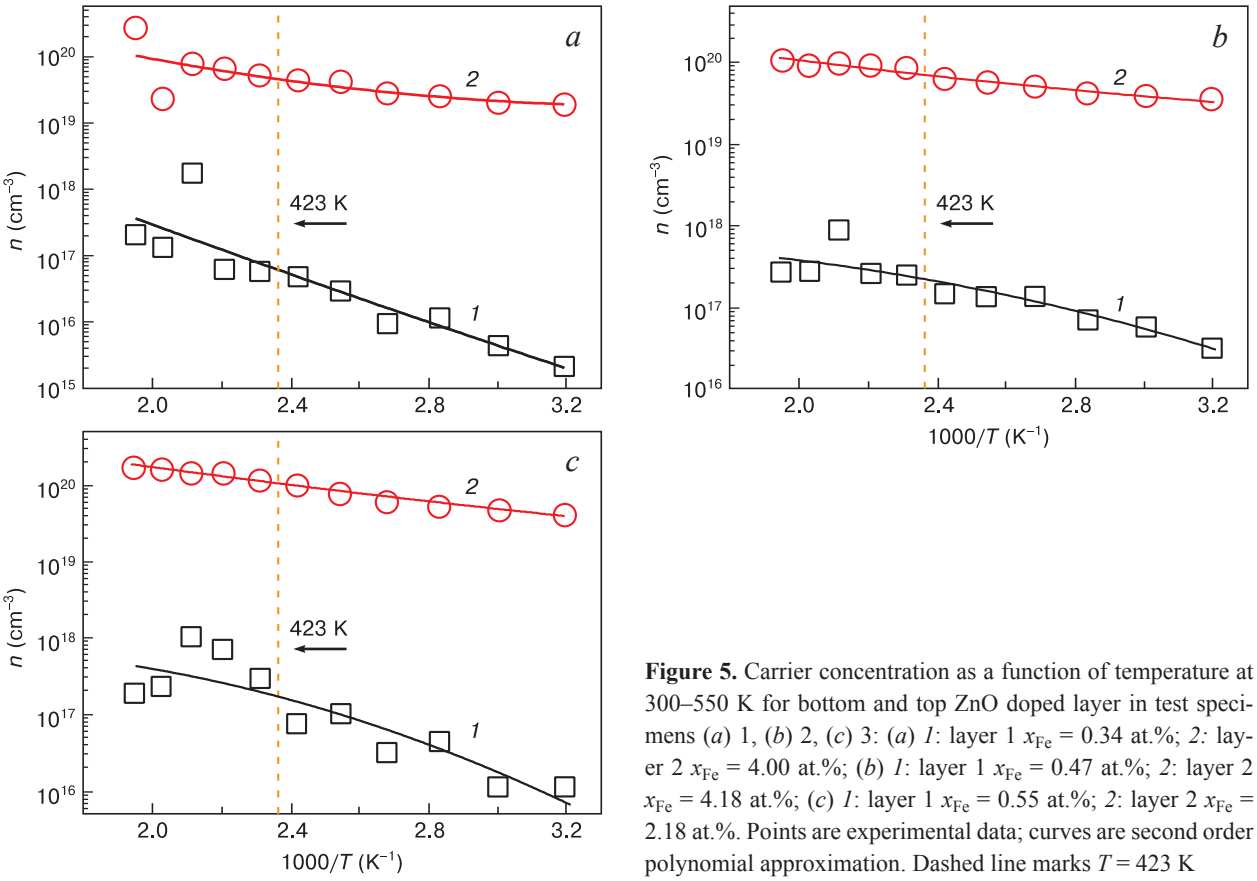

Figure 5. Carrier concentration as a function of temperature at 300–550 K for bottom and top ZnO doped layer in test specimens (*a*) 1, (*b*) 2, (*c*) 3: (*a*) *1*: layer 1 x_{Fe} = 0.34 at.%; *2*: layer 2 x_{Fe} = 4.00 at.%; (*b*) *1*: layer 1 x_{Fe} = 0.47 at.%; *2*: layer 2 x_{Fe} = 4.18 at.%; (*c*) *1*: layer 1 x_{Fe} = 0.55 at.%; *2*: layer 2 x_{Fe} = 2.18 at.%. Points are experimental data; curves are second order polynomial approximation. Dashed line marks T = 423 K

and calculated the difference between the carrier concentrations in the layers Δn for each specimen at 423 K (Fig. 5). The difference was $\Delta n_1 \approx 4.5 \cdot 10^{19}$ cm^{-3}, $\Delta n_2 \approx 7.1 \cdot 10^{19}$ cm^{-3} and $\Delta n_3 \approx 1.0 \cdot 10^{20}$ cm^{-3} for Specimens 1, 2 and 3, respectively. Furthermore, TVE response voltage was studied as a function of temperature for two-layered thin-film Specimen 3 after sequential heating to 498 and 623 K (Fig. 6).

Without dwelling upon the main regularities of the observed TVE changes or causes of TVE growth with temperature and carrier concentration, one can state that the carrier concentration difference between the layers at 423 K is the greatest for Specimen 3 with the lowest iron concentration (2.18 at.%) in the top (heavier doped) zinc oxide layer (Fig. 5*b*). This seems to be the cause of the higher TVE voltage in that specimen. Analysis of the TVE response voltage *vs* temperature curves for the two-layered thin-film Specimen 3 (Fig. 6) showed that the TVE voltage decreased after sequential heating

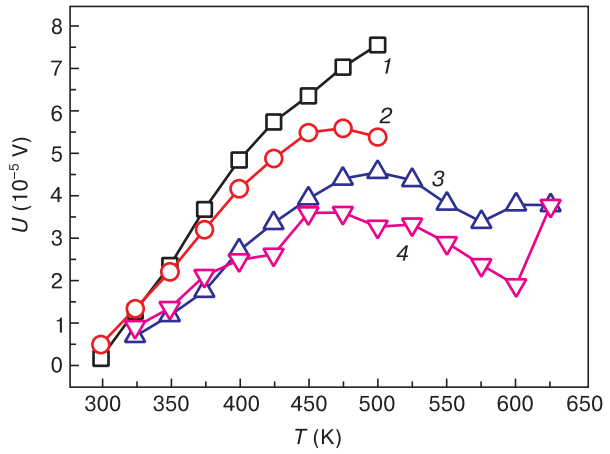

Figure 6. Thermovoltaic response as a function of temperature for two-layered thin-film ZnO/ZnO:Fe Specimen *3* after sequential heating of (*1*, *3*) top and (*2*, *4*) bottom layers to (*1*, *2*) 498 and (*3*, *4*) 623 K

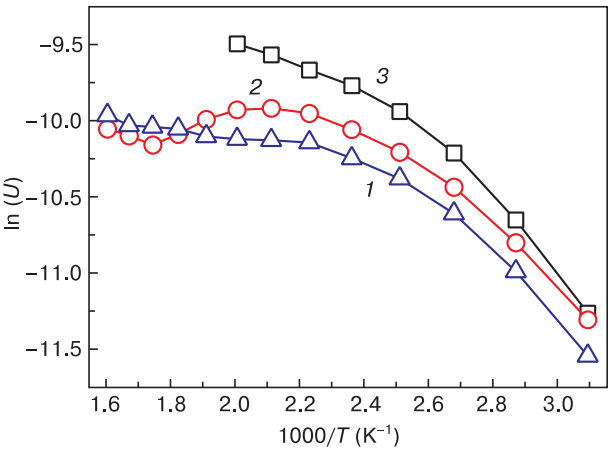

Figure 7. Logarithmic TVE voltage as a function of inverse temperature for thin ZnO/ZnO:Fe films: (*1*) Specimen 1: layer 1 x_{Fe} = 0.34 at.%, layer 2 x_{Fe} = 4.00 at.%); (*2*) Specimen 2: layer 1 x_{Fe} = 0.47 at.%, layer 2 x_{Fe} = 4.18 at.%; (*3*) Specimen 3: layer 1 x_{Fe} = 0.55 at.%, layer 2 x_{Fe} = 2.18 at.%

to 498 and 623 K, same as for Specimens 1 and 2, and sees saturation. These regularities can be accounted for as follows. Uniform heating of a gradient-doped semiconductor specimen triggers carrier diffusion from the higher carrier concentration layer to the lower carrier concentration layer.

Carrier diffusion produces an inner electric field in the specimen causing carrier drift opposite to the carrier diffusion direction. The resultant TVE response is determined by equilibrium between the carrier diffusion and drift currents, i.e., the TVE voltage sees saturation. A decrease in the TVE voltage as a result of sequential heating can be caused by the fact that the time of one measurement which is ~12 h is sufficient for structural relaxation in the specimens, e.g. the number of intrinsic ZnO defects can decrease and the metastable solid solution in the top specimen layer can decompose.

The activation energy of the thermovoltaic response in the synthesized structures was estimated by plotting the temperature functions in the ln $U = f(1/T)$ coordinates (Fig. 7). The initial graph sections (see Fig. 7) are linear and the TVE activation energy was estimated from them to be U = 0.010 ± 0.005 eV. These TVE activation energy data can be logically attributed to carrier mobility fluctuations or hopping conductivity, as observed earlier [34]. Further study of this effect for gradient structures in zinc oxide or other semiconductors will solve a number of questions regarding the physics of this new and attractive phenomenon.

Thus, the origin of the observed TVE is the same (chemical potential gradient) as that of thermo-emf. The difference is that the temperature gradient that causes thermo-emf in specimens is replaced for a doping impurity concentration gradient which generates a thermovoltaic effect voltage even at a zero temperature gradient.

4. Conclusion

A TVE measurement technique for heterogeneous media with doping impurity concentration gradients producing carrier concentration gradients was developed. The TVE in two-layered thin-film zinc oxide specimens with different iron doping impurity concentrations was studied. The strongest TVE response was observed in the specimen with the greatest carrier concentration difference between the layers. The observed TVE saturation was attributed to the establishment of equilibrium between carrier diffusion from the high carrier concentration layer to the low carrier concentration layer and carrier drift due to inner electric field.

Acknowledgements

This work was carried out with support from the Russian Research Foundation, Project No. 24-29-20099.

References

1. Pronin I.A., Averin I.A., Bozhinova A.S., Georgieva A.C., Dimitrov D.C., Karmanov A.A., Moshnikov V.A., Papazova K.I., Terukov E.I., Yakushova N.D. Thermovoltaic effect in zinc oxide inhomogeneously doped with impurities with variable valence. *Pis'ma v zhurnal tekhnicheskoi fiziki*. 2015; 41(19): 22–28. (In Russ.). https://journals.ioffe.ru/articles/42354
2. Takahashi T., Yamada O. Mechanism of voltage generation during phase change of FeS single crystals. *Journal of Physics and Chemistry of Solids*. 1976; 37(2): 161–165. https://doi.org/10.1016/0038-1098(75)90510-4
3. Pronin I.A., Yakushova N.D., Dimitrov D.C., Krasteva L.K., Papazova K.I., Karmanov A.A., Averin I.A., Georgieva A.C., Moshnikov V.A., Terukov E.I. A new type of gas sensors based on the thermovoltaic effect in zinc oxide inhomogeneously doped with impurities of variable valence. *Pis'ma v zhurnal tekhnicheskoi fiziki*. 2017; 43(18): 11–16. (In Russ.). https://doi.org/10.21883/PJTF.2017.18.45028.16754
4. Kaminsky V.V., Solovyov S.M., Sudak N.M., Zaldastanishvili M.I. Detection of the thermovoltaic effect in a heterostructure based on lead telluride. *Pis'ma v zhurnal tekhnicheskoi fiziki*. 2020; (1): 52. (In Russ.). https://doi.org/10.21883/PJTF.2020.01.48866.17834
5. Kaminsky V.V., Kazanin V.V. Thermovoltaic effect in thin-film structures based on samarium sulfide. *Pis'ma v zhurnal tekhnicheskoi fiziki*. 2008; (8): 92–94. (In Russ.). https://journals.ioffe.ru/articles/12044
6. Kaminsky V.V., Solovyov S.M. The emergence of an electromotive force when the valence of samarium ions changes during a phase transition in SmS single crystals. *Fizika tverdogo tela*. 2001; 43(3): 423–426. (In Russ.). https://journals.ioffe.ru/articles/38082
7. Kaminsky V.V., Kazanin M.M., Solovyov S.M., Golubkov A.V. Thermovoltaic effect in heterostructures based on samarium sulfide with the composition $Sm_{1-x}Eu_xS$. *Zhurnal tekhnicheskoi fiziki*. 2012; (6): 142–144. (In Russ.). https://journals.ioffe.ru/articles/10636
8. Egorov V.M., Kaminsky V.V. Endothermic effect when heating semiconductor samarium sulfide. *Fizika tverdogo tela*. 2009; 51(8): 1521–1522. (In Russ.). https://journals.ioffe.ru/articles/2352
9. Kaminsky V.V., Vasiliev L.N., Romanova M.V., Solovyov S.M. The mechanism of occurrence of electromotive force during heating of SmS crystals. *Fizika tverdogo tela*. 2001; 43(6): 997–999. (In Russ.). https://journals.ioffe.ru/articles/38191
10. Kaminsky V.V., Didik V.A., Kazanin M.M., Romanova M.V., Solovyov S.M. Thermovoltaic effect in polycrystalline SmS. *Pis'ma v zhurnal tekhnicheskoi fiziki*. 2009; 35(21): 16–22. (In Russ.). https://journals.ioffe.ru/articles/14013
11. Grevtsev M.A., Kazakov S.A., Kazanin M.M., Kaminsky V.V. Electrical characteristics of a thermovoltaic element based on samarium sulfide. *Zhurnal tekhnicheskoi fiziki*. 2020; 90(10): 1739–1740. (In Russ.). https://doi.org/10.21883/JTF.2020.10.49807.247-19
12. Groshev I., Polukhin I. Samarium sulfide and the latest developments based on it. *Komponenty i tekhnologii*, 2014; (8): 126–133. (In Russ.). https://www.elibrary.ru/item.asp?id = 21884102
13. Patent 2303834 (RF). Thermoelectric generator (variants) and methods of manufacturing a thermoelectric generator. Kaminsky V.V., Golubkov A.V., Kazanin M.M., Pavlov I.V., Solovyov S.M., Sharenkova N.V., 2007. https://rusneb.ru/catalog/000224_000128_0002303834_20070727_C2_RU/
14. Fedotov A.K., Pashkevich A.V., Fedotova J.A., Fedotov A.S., Kołtunowicz T.N., Zukowski P., Ali Arash Ronassi, Fedotova V.V., Svito I.A., Budzyński M. Electron transport and thermoelectric properties of ZnO ceramics doped with Fe. *Journal of Alloys and Compounds*. 2021; 854: 156169. https://doi.org/10.1016/j.jallcom.2020.156169
15. Fedotov A.K., Pashkevich A.V., Khovailo V.V., Kharchenko A.A., Poddenezhny E.N., Bliznyuk L.A., Fedotova V.V. Electrical and thermoelectric properties of ceramics based on ZnO, alloyed with iron and cobalt. *Rossiiskie nanotekhnologii*, 2021; 16: 117–125. (In Russ.). https://doi.org/10.1134/S1992722321030043
16. Winarski D. Synthesis and characterization of transparent conductive zinc oxide thin films by sol-gel spin coating method. Thesis diss. of master science. Graduate College of Bowling Green State University; 2015.
17. Semikina T.V., Komashchenko V.N., Shmyreva L.N. Oxide electronics as one of the directions of transparent electronics. *Elektronika i svyaz'. Tematicheskii vypusk «Elektronika i nanotekhnologii»*. 2010; (3): 20–28. (In Russ.). https://www.researchgate.net/publication/338347890_KPI-transpelectr-2010_3_20_28
18. Hjiria M., El Mir L., Leonardi S.G., Pistone A. Al-doped ZnO for highly sensitive CO gas sensors. *Sensors and Actuators B: Chemical*. 2014; 196: 413–420. https://doi.org/10.1016/j.snb.2014.01.068
19. Hosono H., Ueda K. Transparent Conductive Oxides. Springer, Cham; 2017: 42–51. https://doi.org/10.1007/978-3-319-48933-9_58
20. Ong C.B., Ng L.Y., Mohammad A.W. A review of ZnO nanoparticles as solar photocatalysts: Synthesis, mechanisms and applications. *Renewable and Sustainable Energy Reviews*. 2018; 81(1): 536–551. https://doi.org/10.1016/j.rser.2017.08.020
21. Deng H., Russell J.J., Lamb R.N., Jiang B. Microstructure control of ZnO thin films prepared by single source chemical vapor deposition. *Thin Solid Films*. 2004; 458(1): 43–46. https://doi.org/10.1016/j.tsf.2003.11.288
22. Shinagawa T., Otomo S., Katayama J.-I. Electroless deposition of transparent conducting and (0001)-oriented ZnO films from aqueous solutions. *Electrochemica Acta*. 2007; 53: 1170–1174. https://doi.org/10.1016/j.electacta.2007.03.056
23. Heo Y.W., Norton D.P., Pearton S.J. Origin of green luminescence in ZnO thin film grown by molecular-beam epitaxy. *Journal of Applied Physics*. 2005; 98: 73–81. https://doi.org/10.1063/1.2064308
24. Liu T.Q., Sakurai O., Mizutani N., Kato M. Preparation of spherical fine ZnO particles by the spray pyrolysis method using ultrasonic atomization techniques. *Journal of Materials Science*. 1986; 21(10): 3698–3702. https://doi.org/10.1007/BF02403024
25. Burakov V.S., Tarasenko N.V., Nevar E.A., Nedel'ko M.I. Morphology and optical properties of zinc oxide nanostructures synthesized by the methods of thermal and discharge sputtering. *Zhurnal tekhnicheskoi fiziki*. 2011; 81(2): 89–97. (In Russ.). https://journals.ioffe.ru/articles/10229
26. Nesvetaev D.G., Kaidashev E.M., Puzikov A.S. Pulsed laser spraying of ZnO nanostructures. *Inzhenernyi vestnik Dona*. 2013; (4): 50–55. (In Russ.)

27. Zalesskii V.B., Leonova T.R., Goncharova O.V., Viktorov I.A., Gremenok V.F., Zaretskaya E.P. Production of thin zinc oxide films by reactive magnetron sputtering and investigation of their electrical and optical characteristics. *Physics and chemistry of solid state*. 2005; 6(1): 44–49. (In Russ.)
28. Zhilin D.A., Lyanguzov N.V., Kaidashev E.M. UV photodetector based on nanorods and zinc oxide films. *Inzhenernyi vestnik Dona*. 2013; (4): 55–60. (In Russ.). https://elibrary.ru/item.asp?id = 21452146
29. Samofalova T.V., Semenov V.N. Deposition of thin layers of zinc sulfide from thiourea complexes and their properties. *Kondensirovannye sredy i mezhfaznye granitsy = Condensed Matter and Interphases*. 2016; 18(2): 248–255. (In Russ.). https://journals.vsu.ru/kcmf/article/view/131
30. Lashkova N.A., Maksimov A.I., Matyushkin L.B., Moshnikov V.A., Ryabko A.A., Somov P.A., Tulenin S.S. Local electrophysical properties of conductive ZnO films. *Butlerovskie soobshcheniya*. 2015; 42(6): 48–53. (In Russ.). http://foundation.butlerov.com/bh-2015
31. Gridnev S.A., Kalinin Yu.E., Sitnikov A.V., Stogney O.V. Nonlinear phenomena in nano- and microheterogenic systems. Moscow: Binom, Laboratoriya znanii; 2012. 352 p. (In Russ.)
32. Sitnikov A.V., Makagonov V.A., Kalinin Yu.E., Kushchev S.B., Foshin V.A. Structure and electrical properties of thin-film composites $Co_n(CoO)_{100-n}$. *Zhurnal tekhnicheskoi fiziki*. 2023; 93(11): 1663–1672. (In Russ.). http://dx.doi.org/10.61011/JTF.2023.11.56499.137-23
33. Kanchana S., Chithra M. J., E. Suhashini, Pushpanathan K. Violet emission from Fe doped ZnO nanoparticles synthesized by precipitation method. *Journal of Luminescence*. 2016; 76: 6–14. https://doi.org/10.1016/j.jlumin.2015.12.047
34. Pashkevich A.V., Fedotov A.K., Poddenezhny E.N., Bliznyuk L.A., Fedotova J.A., Basov N.A., Kharchanka A.A., Zukowski P., Koltunowicz T.N., Korolik O.V., Fedotova V.V. Structure, electric and thermoelectric properties of binary ZnO-based ceramics doped with Fe and Co. *Journal of Alloys and Compounds*. 2022; 895(Pt 2): 162621. https://doi.org/10.1016/j.jallcom.2021.162621